Supplementary Information

1 Estimation of deformation

Symmetric and asymmetric deformations for both two and three drop systems (figures 2 and 3) are estimated by (figure 1):

$$D = \frac{P + Q - 2M}{P + Q + 2M} \tag{1}$$

$$AD = \frac{P}{Q} - 1 \tag{2}$$

2 Theory: Two droplet interaction

Consider two droplets of radii, R_1 and R_2 separated by the center to center distance $\tilde{d}$, and subjected to uniform electric field $\tilde{\mathbf{E}}_\mathbf{o}$. Here $\tilde{}$ represents dimensional quantities. The droplets are aqueous and suspended in an insulating oil. The droplet fluids can therefore be modeled as perfect conductors, such that the electric potential inside the droplets is constant. The electric potential in the outer region for each of the droplets, in their local spherical coordinate system, is given by,

$$\tilde{\phi}^{(1)} = \frac{E_o R_1^3 cos\theta}{\tilde{r}^2} - E_o \tilde{r} cos\theta \tag{3}$$

$$\tilde{\phi}^{(2)} = \frac{E_o R_2^3 cos\theta}{\tilde{r}^2} - E_o \tilde{r} cos\theta \tag{4}$$

Where θ is the azimuthal angle, and r is the radial distrance from the local origin of the local spherical coordinate system for each of the droplets. The electric potential due to droplet 2 at $\tilde{r} = \tilde{d}$, i.e. the center of droplet 1 can be written as a multipole expansion as,

$$\tilde{\phi}^{(2\infty)}_{(\tilde{r}=\tilde{d})} = \tilde{\phi}^{(2)}_{(\tilde{r}=d)} + \tilde{r}\left(\frac{\partial\tilde{\phi}^{(2)}}{\partial\tilde{r}}\right)_{\tilde{r}=\tilde{d}} + \frac{\tilde{r}^2}{2}\left(\frac{\tilde{\partial}^2\tilde{\phi}^{(2)}}{\partial\tilde{r}^2}\right)_{\tilde{r}=\tilde{d}} \tag{5}$$

The electric potential due to droplet 2 at $\tilde{r} = \tilde{d}$, the center of droplet 1, acts like an applied potential for droplet 1. Thus if the generic applied potential for droplet 1, due to droplet 2, is given by,

$$\tilde{\phi}^{(1)\infty} = -E_o^{(2)\infty}\tilde{r}cos\theta - \Lambda_o^{(2)\infty}\tilde{r}^2\frac{3\cos^2\theta - 1}{2} + \tilde{\phi}_o^{(2)} \tag{6}$$

then comparing equations 5 and 6 at $\theta = 0$, one can identify,$E_o^{(2)\infty} = -\frac{\partial\tilde{\phi}^{\infty}}{\partial\tilde{r}} = -\left(-\frac{2E_oR_2^3}{\tilde{r}^3}\right)_{\tilde{r}=\tilde{d}} = \left(\frac{2E_oR_2^3}{\tilde{d}^3}\right)$ and $\Lambda_o^{(2)\infty} = -\frac{1}{2}\frac{\partial^2\tilde{\phi}^{\infty}}{\partial\tilde{r}^2} = -\frac{1}{2}\left(\frac{6E_oR_2^3}{\tilde{r}^4}\right)_{\tilde{r}=\tilde{d}} = -\left(\frac{3E_oR_2^3}{\tilde{d}^4}\right)$, while $\tilde{\phi}_o = \tilde{\phi}^{(2)}_{(\tilde{r}=\tilde{d})}$

The coefficients, $E_o^{(1)\infty} = \frac{2E_oR_1^3}{\tilde{d}^3}$ and $\Lambda_o^{(1)\infty} = -\frac{3E_oR_1^3}{\tilde{d}^4}$. Thus the net potential field of the droplet (i) is given by

$$\tilde{\phi}^{(i)} = A_i\frac{cos\theta}{\tilde{r^2}} + B_i\frac{P_2(cos\theta)}{\tilde{r}^3} - (E_o + E_o^{(k)\infty})rcos\theta - \Lambda_o^{(k)\infty}r^2P_2(cos\theta) \quad (7)$$

Where if $i = 1, k = 2$ and vice versa. Imposing vanishing tangential electric field yields, $B_i = R_i^5\Lambda_o^{(k)\infty}$, $A_i = R_i^3(E_o + E_o^{(k)\infty})$.

2.1 Total force on droplet

To check the correctness of calculations, one can get the total z directional force acting on the droplet 1 using the Maxwell stress approach. Since the electric field inside the droplet is absent due to the droplet being a perfect conductor, the electric traction is given by $\tilde{\mathbf{f}}_e^{(i)} = \frac{1}{2}\epsilon_e\left(-\frac{\partial\tilde{\phi}^{(i)}}{\partial r}\right)^2|_{\tilde{r}=\tilde{d}}\mathbf{e_r}$, where $\mathbf{e_r}$ is the unit radial vector. Then, the z direction total force is

$$\tilde{F}_z^{(1)} = \int d\tilde{S}\,\tilde{\mathbf{f}}_e^{(i)}.\mathbf{e}_z = 2\pi R_1^2\int_o^{\pi}\sin\theta d\theta\left(\frac{1}{2}\epsilon_e\left(-\frac{\partial\tilde{\phi}^{(i)}}{\partial r}\right)^2|_{\tilde{r}=\tilde{d}}\cos\theta\right) = \frac{24\pi\epsilon_eR_1^3R_2^3E_o^2}{\tilde{d}^4} \quad (8)$$

This agrees well with the dipolar moment approach (Mhatre and Thaokar, 2015) as well as with the Clausius-Masotti factor approach wherein,

$$\tilde{F}_z^{(1)} = 2\pi\epsilon_eR_1^3CM\nabla(E_\infty^{(1)})^2 = 2\pi\epsilon_eR_1^3(4E_o\Lambda^{(2)\infty}) = 8\pi\epsilon_eR_1^3E_o\left(3\frac{E_oR_2^3}{\tilde{d}^4}\right) = \frac{24\pi\epsilon_eR_1^3R_2^3E_o^2}{\tilde{d}^4} \quad (9)$$

Note that the CM factor (CM=$\frac{\epsilon_i^*-\epsilon_e^*}{\epsilon_i^*+2\epsilon_e^*}$), where the complex permittivity, $\epsilon^* = \epsilon - j\sigma/\omega$, and j is the imaginary unit. For even de-ionized water droplet in an insulating oil, the CM is nearly equal to unity in the low frequency regime (upto kHz of frequency), and approaches unity at much lower frequencies as the conductivity of the water droplet is increased. Note that, for $\theta = 0$, $-\frac{\partial\tilde{\phi}_\infty^{(1)}}{\partial\tilde{r}} = \left(E_o + 2\tilde{r}\Lambda_0^{(2)\infty}\right)$, such that, $\nabla E_\infty^2 = \frac{\partial E_\infty^2}{\partial\tilde{r}}|_{\tilde{r}=0} = \frac{\partial}{\partial\tilde{r}}\left(2(E_o + 2\tilde{r}\Lambda_0^{(2)\infty})(2\Lambda_0^{(2)\infty})\right) = 4E_o\Lambda_0^{(2)\infty}$ at $\tilde{r} = 0$, the center of droplet 1.

2.2 Electric fields at interacting poles

Electric field at the two interaction poles for droplet 1 and droplet 2 are given by,

$$\left(-\frac{\partial\tilde{\phi}^{(1)}}{\partial\tilde{r}}\right)(\theta = \pi) = -3E_o - \frac{6E_oR_2^3}{\tilde{d}^3} - \frac{15E_oR_1R_2^3}{\tilde{d}^4} \quad (10)$$

$$\left(-\frac{\partial\tilde{\phi}^{(2)}}{\partial\tilde{r}}\right)(\theta=0) = 3E_o + \frac{6E_oR_1^3}{\tilde{d}^3} + \frac{15E_oR_2R_1^3}{\tilde{d}^4} \tag{11}$$

Thus the electric field at the interacting pole of the smaller droplet 2 is greater than that for the bigger droplet 1. The cone angle though is determined by the deformation, and it is therefore useful to investigate the deformation at the interacting poles.

2.3 Curvature and Maxwell forces

The shape of the droplet $i = 1, 2$, is given by $\tilde{r}_s^i = R_i + \Sigma_{l=1}^{l=4}\tilde{s}_1^i P_l(cos\theta)$. The curvature is given by $\tilde{C}_i = 2/R_i + \Sigma_{l=1}^{l=4}\tilde{s}_l^i\,(l(l+1)-2)\,P_l(cos\theta)$. Thus the curvature stress, which acts normal to the sphere, is,

$$\gamma\left[\frac{2}{R_i} + 4\frac{\tilde{s}_2^{(i)}}{R_i^2}P_2(cos\theta) + 10\frac{\tilde{s}_3^{(i)}}{R_i^2}P_3(cos\theta) + 18\frac{\tilde{s}_4^{(i)}}{R_i^2}P_4(cos\theta)\right]. \tag{12}$$

This balances the electric stress $\tilde{f}_e^i = \frac{1}{2}\epsilon_e(\tilde{E}_r^{(i)})^2$ equation (7) and the hydrodynamic stress.

2.3.1 Centre of mass motion and unsteady droplet deformation

The center of mass motion and unsteady deformation is determined by simultaneously solving for the velocity field. The Gegenbauer functions are used to describe stream functions and conditions of velocity continuity, stress balance and kinematic boundary conditions to determine the evolution of the separation d(t) and the deformation modes $s_l(t)$. The methodology is similar to that described in our earlier works (Thaokar, 2012). We consider for simplicity, that the droplets do not interact hydrodynamically. Thus the hydrodynamics of each of the droplet is considered to be that of a single droplet in electric field. The velocity stream functions $\psi_{i,e}$, are expressed in terms of Gegenbauer functions $G_i(\cos theta)$, and then velocities, hydrodynamic stresses are calculated using the appropriate definitions.

$$\psi_e = G_2\left(\frac{C_{2ae}}{r} + C_{2be}r\right) + G_3\left(\frac{C_{3ae}}{r^2} + C_{3be}\right) + G_4\left(\frac{C_{4ae}}{r^3} + \frac{C_{4be}}{r}\right) + G_5\left(\frac{C_{5ae}}{r^4} + \frac{C_{5be}}{r^2}\right) \tag{13}$$

$$\psi_i = G_2\left(C_{2ai}r^4 + C_{2bi}r^2\right) + G_3\left(C_{3ai}r^5 + C_{3bi}r^3\right) + G_4\left(C_{4ai}r^6 + C_{4bi}r^4\right) + G_5\left(C_{5ai}r^7 + C_{5bi}r^5\right)$$

The unknown coefficients are estimated using the boundary conditions,namely velocity continuity, normal and tangential stress balances and the kinematic condition give the evolution equations for both the center of mass motion of the droplets, and the deformation modes. The orthonganality condition for Legendre polynomials is used. Axisymmetry is assumed in the calculations.

The equation of motion leads to the following equation for the variation of change in the inter droplet distance with time

$$d(t) = \left(d_o^5 - \frac{(60\chi^2(1+\chi)(1+\lambda)}{(2+3\lambda)} t \right)^{1/5}. \tag{14}$$

. Here, the distances are non-dimensionalised by R_1, and $\chi = R_2/R_1$. the time is non-dimensionalised by $\mu_e/\epsilon_e E_o^2$. $\lambda = \mu_i/\mu_e$. The coefficients associated with Legendre Polynomials, evolve as a first order equation with time constants, T_{s_l}, associated with the deformation mode l with amplitude s_l,

$$\frac{d}{dt} s_l(t) = -\frac{s_l(t)}{T_{s_l}} + A_l \tag{15}$$

where A_l is a constant associated with the evolution equation for the shape modes. The time constants are listed below,

$$T_{s_2^{(2)}} = \frac{Ca\chi(3+2\lambda)(16+19\lambda)}{40(1+\lambda)} \tag{16}$$

$$T_{s_3^{(2)}} = \frac{Ca\chi(10+11\lambda)(19+16\lambda)}{280(1+\lambda)} \tag{17}$$

$$T_{s_4^{(2)}} = \frac{Ca\chi(11+10\lambda)(16+17\lambda)}{360(1+\lambda)} \tag{18}$$

$$T_{s_2^{(1)}} = \frac{Ca(3+2\lambda)(16+19\lambda)}{40(1+\lambda)} \tag{19}$$

$$T_{s_3^{(1)}} = \frac{Ca(10+11\lambda)(19+16\lambda)}{280(1+\lambda)} \tag{20}$$

$$T_{s_4^{(1)}} = \frac{Ca(11+10\lambda)(16+17\lambda)}{360(1+\lambda)}. \tag{21}$$

Here, the capillary number $Ca = R_1\epsilon_e E_o^2/\gamma$. It is convenient to express deformation in terms of the symmetric and asymmetric degrees of deformation.

$$D = \frac{rs(\frac{\pi}{2}) - rs(0)}{rs(\frac{\pi}{2}) + rs(0)} = \frac{3}{4}s_2 + \frac{5}{16}s_4 \tag{22}$$

$$AD - 1 = \frac{r_s(0)}{rs(\pi)} - 1 = 2s_3 \tag{23}$$

One can thus construct the unsteady D and AD trajectories for the two drops.

2.3.2 Quasi-Steady state deformation

The estimates of deformation can be obtained by balancing the electric stress and the curvature stress that gives the instantaneous quasi-steady shape of the

droplets for given positions of the droplets. Thus we get, the quasi-steady state deformation as

$$D^{(2)} = \frac{9Ca\chi^2}{16}\left(1 + \frac{1}{4d^3}\right) \tag{24}$$

$$AD^{(2)} = -\frac{27}{5}Ca\frac{\chi^3}{d^4} \tag{25}$$

$$D^{(1)} = \frac{9Ca}{16}\left(1 + \frac{\chi^3}{4d^3}\right) \tag{26}$$

$$AD^{(1)} = -\frac{27}{5}Ca\frac{\chi^3}{d^4} \tag{27}$$

It is seen that while the bigger droplet deforms more due to its bigger size, the deformation due to interaction is greater for the smaller droplet (the second term in the bracket of equations 24 and 26). Although, $AD^{(1)} = AD^{(2)}$, it should be mentioned that AD could lead to formation of asymmetric conical tips at the interacting poles of the two droplets.

3 Theory: Three droplet interaction

Consider a three droplet system of radii, $R_1 = R_3$ which flank droplet 2 or radius R_2. The center to center distance between droplets 1 and 2 is the same as between 2 and 3 and is equal to d, and the three droplets are subjected to uniform electric field E_0. The droplet 2 remains stationary. The droplet 1 experiences, $E_o^{(2)\infty} = \frac{2E_oR_2^3}{\tilde{d}^3}$, $\Lambda_o^{(2)\infty} = -\frac{3E_oR_2^3}{\tilde{d}^4}$, $E_o^{(3)\infty} = \frac{2E_oR_3^3}{(2\tilde{d})^3}$ and $\Lambda_o^{3\infty} = -\frac{3E_oR_3^3}{(2d)^4}$, as an effective applied field due to droplets 2 and 3.

3.1 Total force on droplet

The total z directional force acting on the droplet 1 is,

$$\tilde{F}_z^{(1)} = 2\pi\epsilon R_1^3\nabla E_\infty^2 = 8\pi\epsilon_e R_1^3 E_o(\Lambda_o^{(2)\infty} + \Lambda_o^{(3)\infty}) = \frac{3\pi\epsilon E_o^2 R_1^6(1+16\chi^3)}{2\tilde{d}^4} \tag{28}$$

3.2 Electric fields at interacting poles

Electric field at the two interaction poles for droplet 1 and droplet 2 are given by,

$$-\left(\frac{\partial\tilde{\phi}^{(1)}}{\partial\tilde{r}}\right)(\theta=\pi) = -3E_o - \frac{6E_oR_2^3}{\tilde{d}^3} - \frac{6E_oR_1^3}{(2\tilde{d})^3} \tag{29}$$

$$\left(-\frac{\partial\tilde{\phi}^{(2)}}{\partial\tilde{r}}\right)(\theta=0) = 3E_o + \frac{12E_oR_1^3}{\tilde{d}^3} \tag{30}$$

Thus the electric field at the interacting pole of the smaller droplet is greater than that for the bigger droplet.

3.2.1 Center of mass motion and unsteady deformation

The variation of the inter droplet distance with time is given by

$$d(t) = \left(d_o^5 - \frac{30(1+2\chi^3)(1+\lambda)}{(2+3\lambda)} t \right)^{1/5} \tag{31}$$

The time constants associated with the deformation modes are given by,

$$T_{s_2^{(2)}} = \frac{Ca\chi(3+2\lambda)(16+19\lambda)}{40(1+\lambda)} \tag{32}$$

$$T_{s_3^{(2)}} = \frac{Ca\chi(10+11\lambda)(19+16\lambda)}{280(1+\lambda)} \tag{33}$$

$$T_{s_4^{(2)}} = \frac{Ca\chi(11+10\lambda)(16+17\lambda)}{360(1+\lambda)} \tag{34}$$

$$T_{s_2^{(1)}} = \frac{Ca(3+2\lambda)(16+19\lambda)}{40(1+\lambda)} \tag{35}$$

$$T_{s_3^{(1)}} = \frac{Ca(10+11\lambda)(19+16\lambda)}{280(1+\lambda)} \tag{36}$$

$$T_{s_4^{(1)}} = \frac{Ca(11+10\lambda)(16+17\lambda)}{360(1+\lambda)} \tag{37}$$

3.2.2 Quasi-steady state deformation

The quasi-steady state deformation are given as

$$\begin{aligned} D^{(2)} &= \frac{9Ca\chi^2}{16}\left(1+\frac{8}{d^3}\right) \\ AD^{(2)} &= 0 \\ D^{(1)} &= \frac{9Ca}{16}\left(1+\frac{1+8\chi^3}{2d^3}\right) \\ AD^{(1)} &= -\frac{27}{80}Ca\frac{1+16\chi^3}{d^4} \end{aligned}$$

Thus it shows that while the bigger droplet deforms more due to its bigger size, the deformation due to interaction is greater for the smaller droplet. Interestingly $AD^{(2)} = 0$, since for the central droplet, flanked by two equal sized, equally separated droplets, the deformation is symmetric. $AD^{(2)}$, the deformation of the outer two droplets increases with Ca. It should be mentioned that AD could lead to formation of asymmetric conical tip at the interacting poles of the two droplets. In three drop system drop 1 (R_1) and drop 2 (R_2) are considered for the analysis.

3.3 Renormalisation of critical electric field for three droplet system

The electric field experienced by the central droplet in n droplet systems is given by

$$E = E_o \left(1 + 2\frac{2R_1^3}{\tilde{d}^3} + 2\frac{2R_1^3}{(2\tilde{d})^3} + 2\frac{2R_1^3}{(3\tilde{d})^3} + \cdots\right) = E_o \left(1 + 2\frac{2R_1^3}{\tilde{d}^3}\sum_{n=1}^{\infty}\frac{1}{n^3}\right) \quad (38)$$

Noting that $\sum_{n=1}^{\infty}\frac{1}{n^3} = \zeta(3)$, and zeta function $\zeta(3) = 1.2$. Relating $\frac{4/3\pi R_1^3}{\tilde{d}^3} = \phi_v$, where ϕ_v here is the volume fraction of the dispersed phase, we get the reduction in critical electric field due to a chain of n droplets.

3.4 Discussion of results

Figures 4 and 5 denote theoretically obtained variation of electric field at the adjacent poles (E_n^p) and symmetric and asymmetric deformation for two droplet system with time. It is observed that E_n^p of drop 2 (R_2) at the time of contact increases significantly faster than that of drop 1 (R_2) which is qualitatively in line with numerical simulations. Figures 5(a) and 5(b) shows the evolution of D and AD with time. It is observed that both D and AD show higher deformation of drop 1 initially. However the rate of increase of deformation near contact for drop 2 is significantly higher. This is also predicted by numerical simulations and experimental observations.

Figure 6 shows the variation of the theoretically obtained electric field at the adjacent poles (E_n^p) for three droplet system with time. It is observed that E_n^p of drop 2 (R_2) at the time of contact increases significantly faster than that of drop 1 (R_2). Numerical simulations predict as such. Observations analogous to two drop system are also seen in case of three drop system shown in figure 7(a). In figure 7(b), however, comparison of only AD of drop 1 is plotted as AD of drop 2 is always 0 on account of perfectly symmetric position and subsequent symmetric deformation.

4 Estimation of tangential stress

The tangential electric field, and thereby electrohydrodynamic flows are negligible with our chosen conductivity ratio ($\sigma_r = 0.001$) as the leaky-dielectric system modeled in this work is extended to perfectly conducting perfect dielectric system. To validate this a test case is simulated with $R_1 = R_3 = 1$ and $R_3 = 0.5$ with $Ca = 0.1$.
Both normal and tangential stress distributions are also plotted (figure 8) across all the nodes of the drops for both $t = 0$ and $t = contact$ as shown in figure 8. It shows that PC modeling used for our numerical analysis with σ_r and Q and

taking limiting case is accurate and tangential stresses are only of order of 0.1 indicating numerical accuracy.

5 Velocity, pressure and Maxwell stress distribution

Velocity field, electric stress (Maxwell stress) distribution and pressure profiles have been plotted for two three-droplet systems (figure 9).
In both two and three droplet systems, uncharged, perfectly conducting drops are placed in an uniform electric field E_0 in a perfectly dielectric medium. The droplets behave like a neutral conductor sphere and in presence of the externally applied electric field it gets polarized such that the positive and negative charges migrate towards the north and south poles respectively to negate the internal field lines. The charge density on the interface is given by $\tilde{q_s} = \epsilon_0 \epsilon_e \tilde{E_n}$. Thus the normal electric field in our calculations is associated with corresponding free surface charge density given by q = $\epsilon_0 \epsilon_e E_n$. Maxwell stress corresponding to normal electric field is plotted in figure 9(c).
The bridge connecting two droplets break on account of competition between azimuthal and meridional curvatures (Roy et al., 2019). It was observed that when the strength of electric field is greater than the critical value ($Ca > Ca_c$) the azimuthal curvature dominates leading to increased pressure at the bridge which causes non-coalescence. When strength of electric field is below the critical value ($Ca < Ca_c$) the meridional curvature dominates leading to decreased pressure in the bridge which causes the droplets to coalesce. These are shown in figures 9(a) and 9(b).

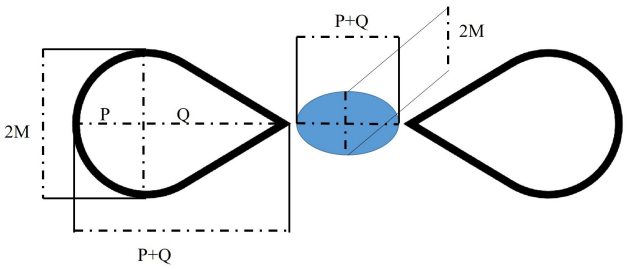

Figure 1: Estimation of symmetric and asymmetric deformation

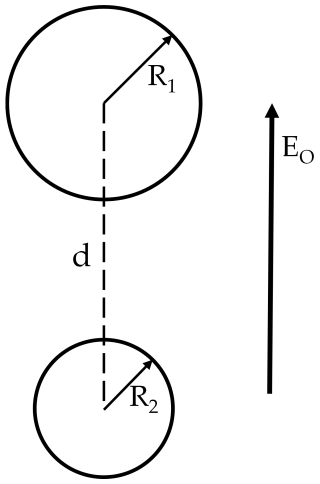

Figure 2: Two droplet system.

References

Mhatre, S. and Thaokar, R. (2015). Electrocoalescence in non-uniform electric fields: An experimental study. *Chemical Engineering and Processing: Process Intensification*, 96:28–38.

Roy, S., Anand, V., and Thaokar, R. M. (2019). Breakup and non-coalescence mechanism of aqueous droplets suspended in castor oil under electric field. *Journal of Fluid Mechanics*, 878:820–833.

Thaokar, R. (2012). Dielectrophoresis and deformation of a liquid drop in a non-uniform, axisymmetric ac electric field. *The European Physical Journal E*, 35(8):1–15.

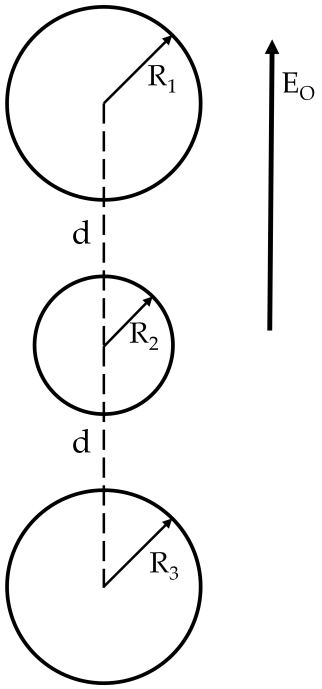

Figure 3: Three droplet system.

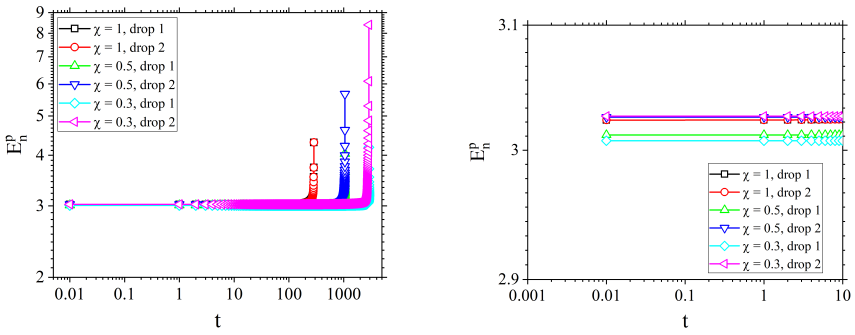

Figure 4: (a) Theoretically obtained variation of electric field at the adjacent poles (E_n^p) for two-droplet system with non dimensional time (t) (b) Closer look at variation of electric field from time $t = 0.01$ to $t = 1$.

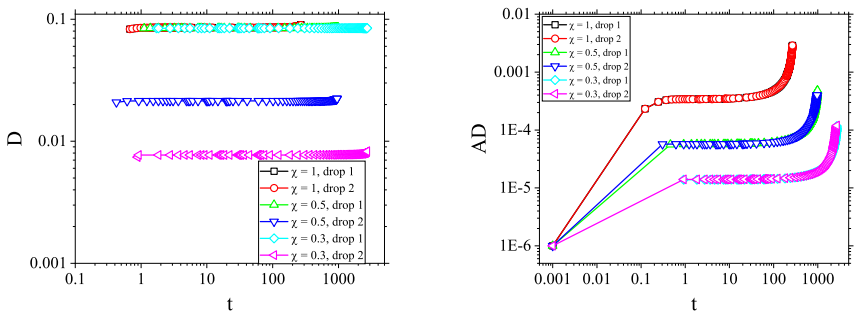

a b

Figure 5: (a) Theoretically obtained variation of symmetric deformation of individual droplets under electric field with time (t) in two droplet system (b) Theoretically obtained variation of asymmetric deformation of individual droplets under electric field with time (t) in two droplet system.

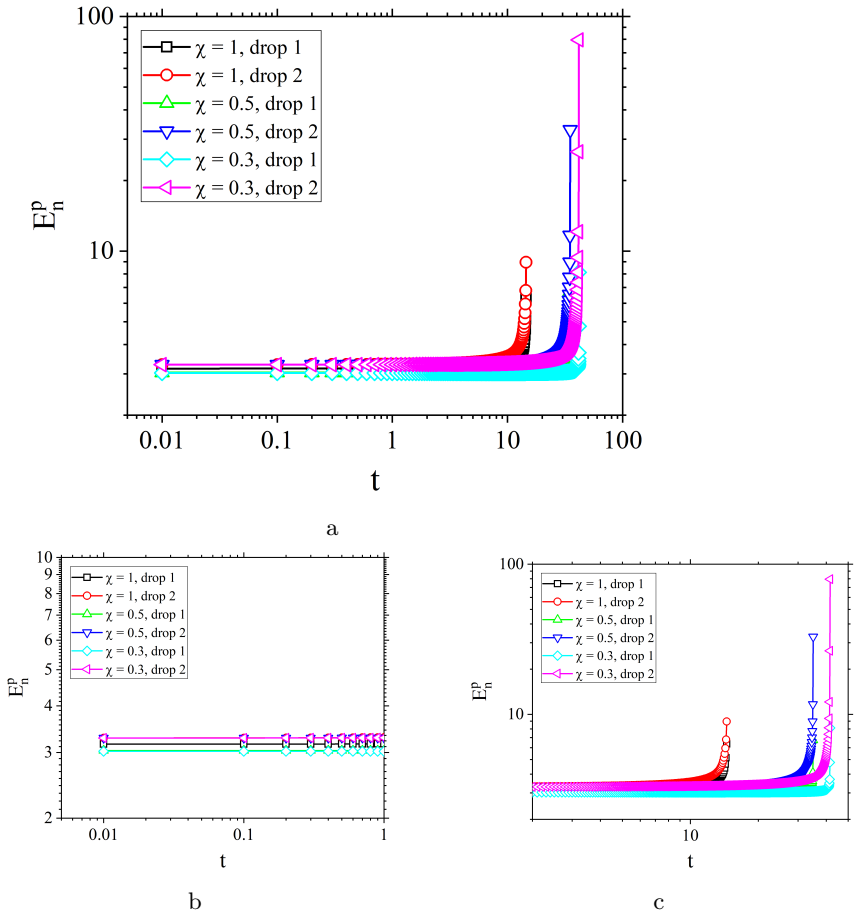

Figure 6: (a) Theoretically obtained variation of electric field at the adjacent poles (E_n^p) for three droplet system with non dimensional time (t) (b) Closer look at variation of electric field from time $t = 0.01$ to $t = 1$ (c) Closer look at variation of electric field from time $t = 10$ to $t = 40$.

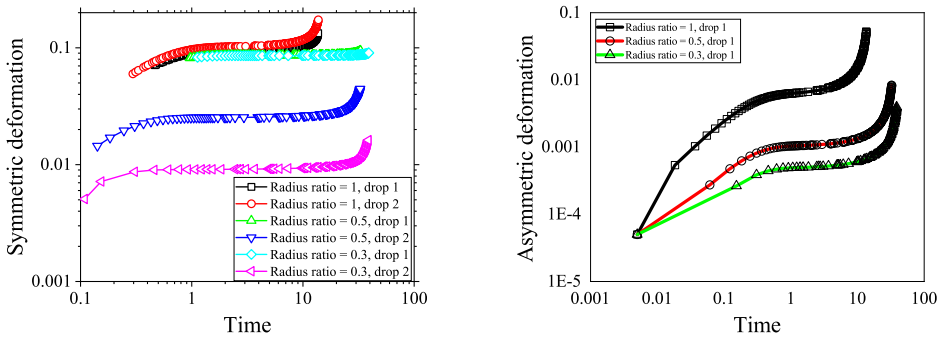

a b

Figure 7: (a) Theoretically obtained variation of symmetric deformation (D) of individual droplets under electric field with time in three droplet system (b) Theoretically obtained variation of asymmetric deformation (AD) of individual droplets under electric field with time in three droplet system.

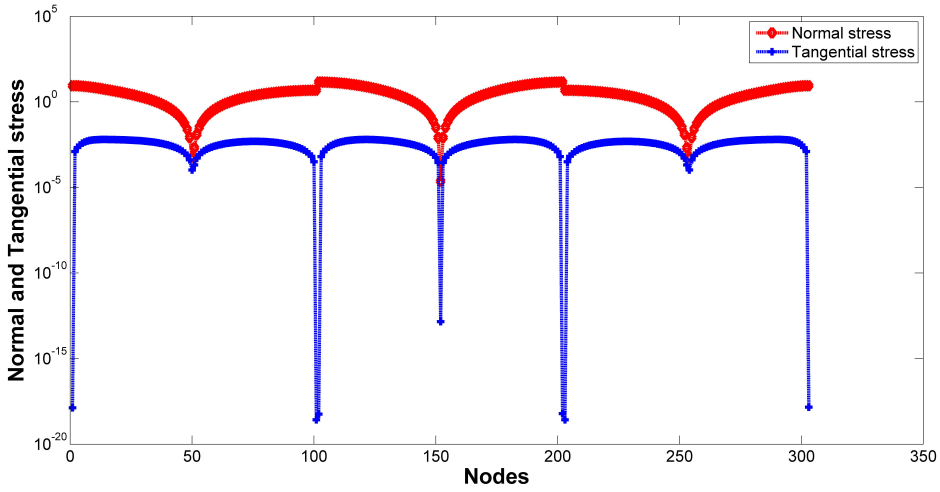

a

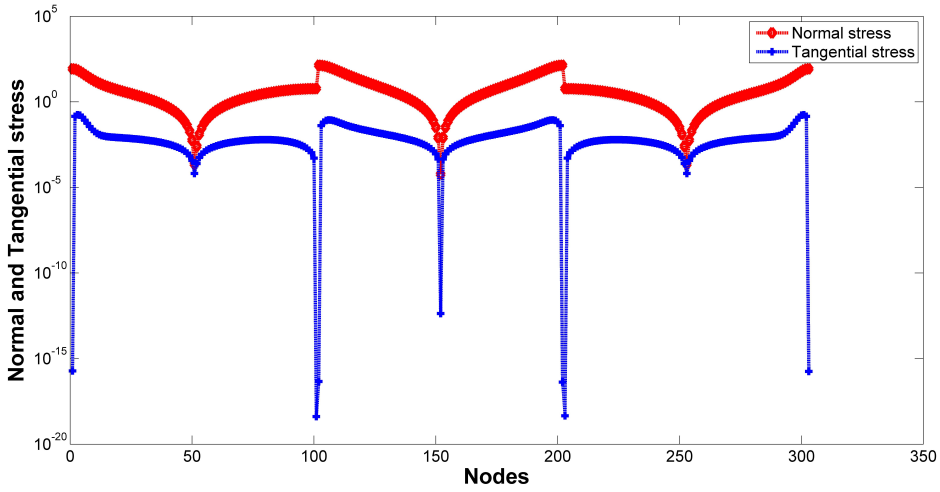

b

Figure 8: Normal and tangential stress distribution for a 3 drop setup ($R_1 = R_2 = 1$ and $R_3 = 0.5$ with $Ca = 0.1$ and center to center distance between the outer and inner drop=2) at: (a) $t = 0$ and (b)$t = contact$.

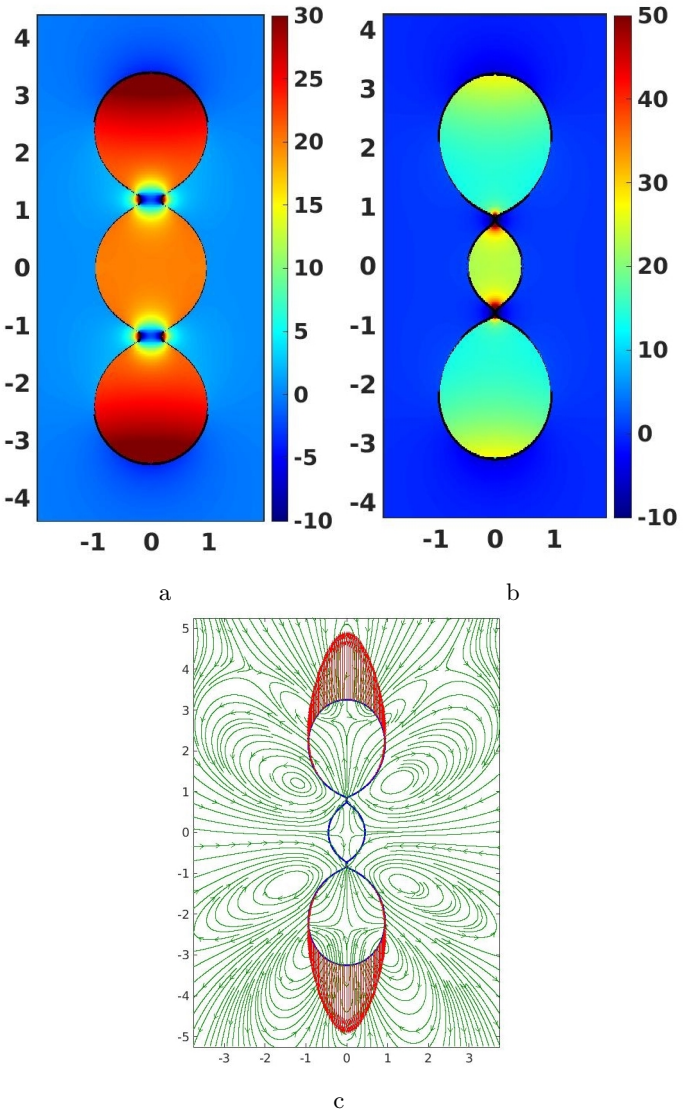

Figure 9: (a)Pressure profile for a system of three drops with $R_1 = R_2 = R_3 = 1$ and $Ca = 0.1$ exhibiting coalescence, (b)Pressure profile for a system of three drops with $R_1 = R_3 = 1$ and $R_2 = 0.5$ and $Ca = 0.1$ exhibiting non-coalescence, and (c)Velocity (in green) and Maxwell stress profile (in red) for a system of three drops with $R_1 = R_3 = 1$ and $R_2 = 0.5$ and $Ca = 0.1$ exhibiting non-coalescence.